Available online at www.sciencedirect.com
SCIENCE DIRECT®
Composites Science and Technology 63 (2003) 1543–1550
COMPOSITES SCIENCE AND TECHNOLOGY
www.elsevier.com/locate/compscitech

# Transverse mechanical properties of single-walled carbon nanotube crystals. Part I: determination of elastic moduli

E. Saether[a,*], S.J.V. Frankland[b], R.B. Pipes[c]

[a]NASA Langley Research Center, MS 240, Hampton, VA 23681, USA
[b]National Institute of Aerospace, NASA Langley Research Center, Hampton, VA 23666, USA
[c]Polymer Engineering, University of Akron, Akron, OH 44325, USA

Received 16 August 2002; received in revised form 16 September 2002; accepted 15 October 2002

**Abstract**

Carbon nanotubes naturally tend to form crystals in the form of hexagonally packed bundles. An accurate determination of the effective mechanical properties of nanotube bundles is important in order to assess potential structural applications such as reinforcement in future composite material systems. Although the intratube axial stiffness is on the order of 1 TPa due to a strong network of carbon–carbon bonds, the intertube interactions are controlled by weaker, nonbonding van der Waals forces which are orders of magnitude less. A direct method for calculating effective material constants is implemented in the present study. The Lennard–Jones potential is used to model the nonbonding cohesive forces. A complete set of transverse moduli is obtained and shown to exhibit a transversely isotropic constitutive behavior. The predicted elastic constants obtained using the direct method are compared with available published results obtained from other methods.
Published by Elsevier Ltd.

*Keywords:* B. Mechanical properties; Composites; Carbon nanotubes; Bundles

## 1. Introduction

Future nanostructured composite materials are expected to incorporate carbon nanotube reinforcement either dispersed individually or as nanofilamentary bundles or ropes yielding unprecedented mechanical properties. A carbon nanotube is a cylindrical molecule composed of single or multiple walls of graphene sheets. These sheets are, in turn, composed of hexagonal units or graphene rings of carbon atoms that are bonded through highly stable $sp^2$ hybridized orbitals. A typical carbon nanotube is schematically depicted in Fig. 1, while Fig. 2 contains a cross-section of a bundle ensemble of individual nanotubes obtained through transmission electron microscopy (TEM) [1].

Numerous studies have been made to analytically and experimentally determine the elastic properties of individual nanotubes. Axial Young's moduli on the order of 1 TPa have been measured using atomic force microscopy (AFM) [2] and thermal vibrations [3]. Analytical studies have utilized ab initio calculations [4], tight-binding methods [5], molecular dynamic simulations (MD) [6] and lattice dynamics [7,8]. These elastic properties are entirely based on the strong intratube valence forces of the carbon–carbon bonds.

Nanotube ensembles, however, typically form hexagonally packed crystal configurations in which the intertube force interactions are due exclusively to nonbonding van der Waals effects which are much weaker than the valence forces and are highly nonlinear. Less consideration has been given to the transverse mechanical properties of nanotube bundles which depend on a good description of these non-bonding interactions. These intertube cohesive properties are of special interest for use in predicting the properties of carbon nanotube polymer composites [9] and fibers of helical nanotube arrays [10]. Selected moduli of nanotube bundles have been calculated with a continuum model based on the integrated average of the discrete Lennard–Jones potential [11], MD simulation using the Tersoff–Brenner potential [12] and lattice dynamic methods [13,14].

* Corresponding author. Tel.: +1-757-864-8079; fax: +1-757-864-8912.
*E-mail address:* e.saether@larc.nasa.gov (E. Saether).

0266-3538/03/$ - see front matter Published by Elsevier Ltd.
doi:10.1016/S0266-3538(03)00056-3

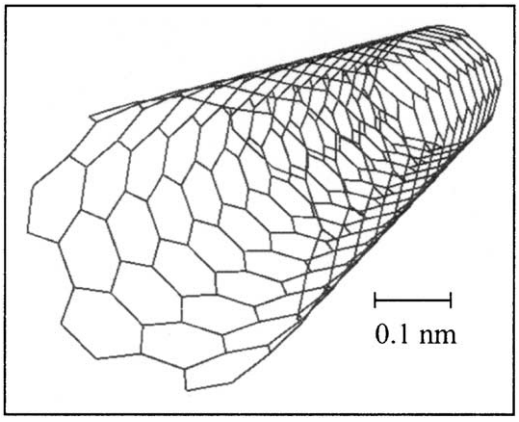


Fig. 1. Single-walled nanotube.

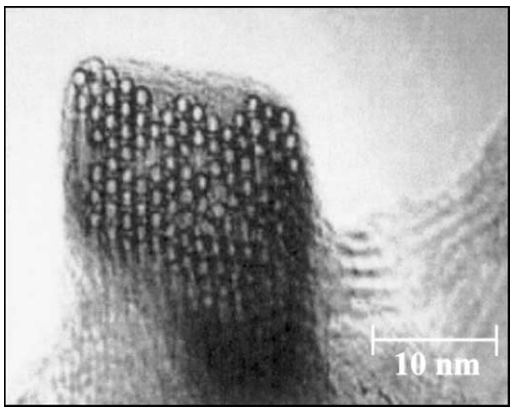


Fig. 2. Typical nanotube bundle [1].

For the present study, a direct summation of atom-pair potentials is used to avoid any simplifications made to the nonlinear van der Waals interactions. Because the fundamental constituents of nanotube bundles are only resolvable at nanometer length scales, analyses to predict macroscopic properties must necessarily merge concepts and techniques from continuum elasticity theory and discrete molecular simulation. The basic approach of subjecting a molecular ensemble to applied strain modes and recovering effective moduli from energy measures has been used in molecular dynamic simulations [15,16]. The methodology developed herein combines a unit cell continuum model with molecular static calculations to determine effective moduli in aligned carbon nanotube bundles.

The Lennard–Jones potential is utilized to simulate the van der Waals interaction forces among carbon atom-pairs in aligned carbon nanotube arrays. An achiral "zig-zag" configuration is assumed for the carbon nanotubes with 12 graphene units around the circumference. Using the standard Hamada index notation [25], this configuration is referred to as a (12,0) nanotube. The resulting tube radius is assumed small such that the cross-section can be considered rigid.

The objective of this work is to formulate a model that combines principles from continuum elasticity and molecular mechanics to predict the off-axis elastic properties of carbon nanotube bundles. The calculated moduli are shown to exhibit a transverse isotropy which is anticipated for a material possessing hexagonal symmetry. The predicted moduli are compared with available published data.

## 2. Material constitutive relationship

The force field within a nanotube crystal consists of a combination of strong linear bonding forces acting within the nanotube and weak non-bonding forces acting between adjacent nanotubes. This disparity between the magnitude of interatomic forces leads to a highly anisotropic constitutive relation. The minimum energy configuration of a nanotube crystal assumes a hexagonal packing arrangement. Considered as a solid material, the hexagonal symmetry shown in Fig. 3 would be expected to yield a material exhibiting transverse isotropy [17]. The coordinate system assumed for individual nanotubes and the form of the stress–strain relation is shown in Fig. 4.

A transversely isotropic material is defined by five independent parameters, $C_{11}$, $C_{12}$, $C_{44}$, $C_{22}$ and $C_{23}$. For the transverse plane in a nanotube bundle, only two

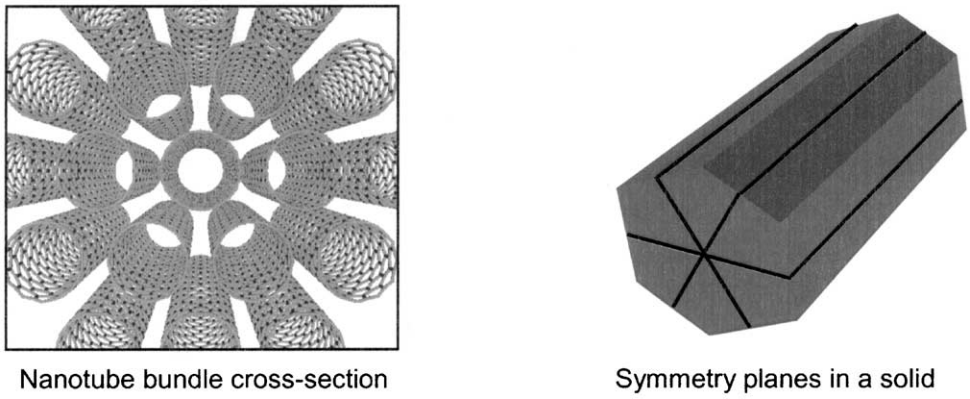


Fig. 3. Hexagonal symmetry in a nanotube bundle considered as a solid.

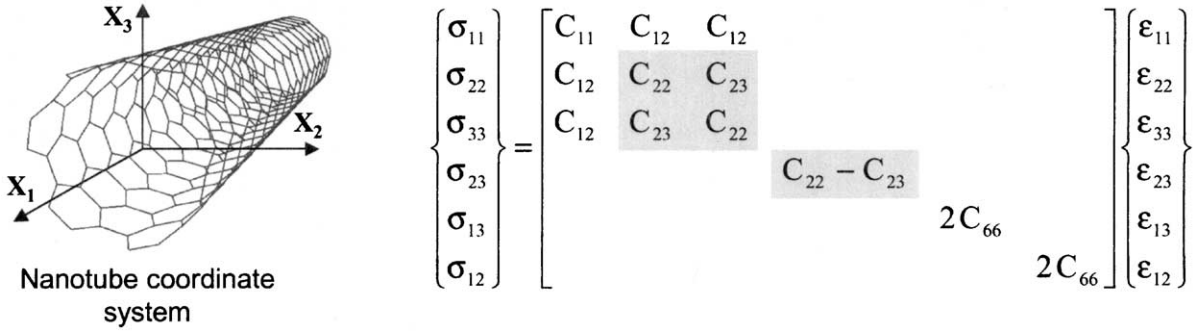


Fig. 4. Nanotube coordinate system and constitutive law for transverse isotropy.

independent elastic constants are required to describe the isotropic properties. These constants are given by the $C_{22}$ and $C_{23}$ stiffness coefficients, which are highlighted in the constitutive relation presented in Fig. 4.

Additional relationships between the material constants in the transverse plane for a hexagonal system are given by

$$K_{23} = (C_{22} + C_{23})/2$$
$$G_{23} = (C_{22} - C_{23})/2 \quad (1)$$

where $K_{23}$ and $G_{23}$ are the transverse bulk and shear moduli, respectively.

Because the axial stiffness of individual nanotubes has been extensively reported in the literature, the current effort will focus on completing the mechanical description by predicting the elastic moduli in the transverse plane.

## 3. Modified unit cell formulation

In micromechanical analyses, the method of unit cells has been used to determine the effective properties of heterogeneous materials by identifying and analyzing convenient domains of repeating microstructure. In the current study, a repeating unit of nanotubes is defined and subjected to continuous field deformation modes, during which the system energy is calculated. Because the potential energy of the system is due to atom-pair interactions between adjacent nanotubes, a special type of boundary condition is imposed which is termed 'periodic'. Under periodic boundary conditions (PBC's), cells of nanotubes in the transverse plane and nanotube segments in the axial dimension are treated as images of the constituents within the cell and used in the calculation of potential energy. This permits interactions between atom-pairs across the boundary to avoid introducing discontinuities in the force field. In general, these conditions ensure conservation of mass and energy, avoid surface or boundary effects, and mathematically give the primary unit cell a strict periodicity such that it can be considered to represent an infinite ensemble of molecules [18]. By combining concepts from continuum elasticity and molecular dynamics, these representative units will be referred to herein as 'PBC-unit cells'. Fig. 5 shows an assemblage of a square PBC-unit cell of nanotubes with surrounding image tubes that are required in applying periodic boundary

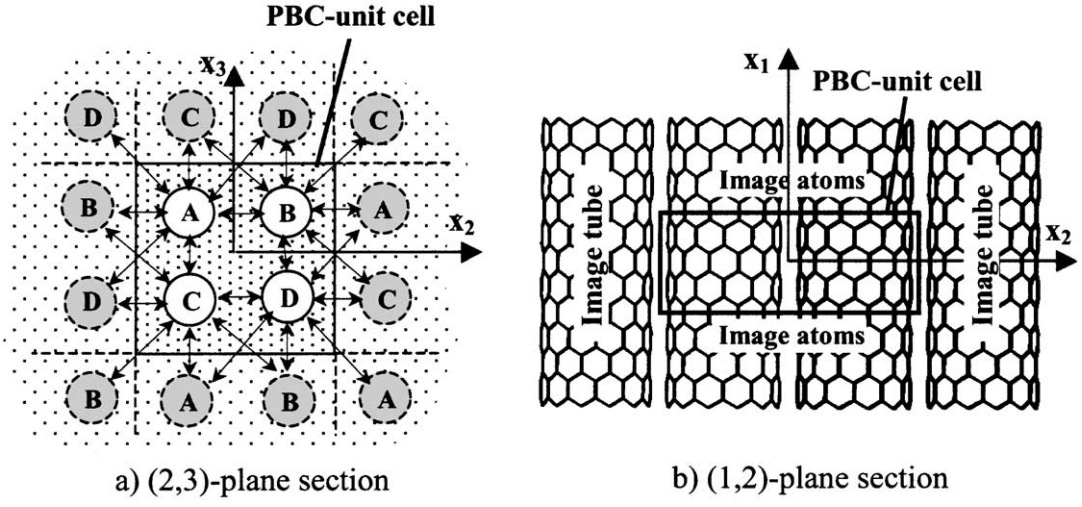


Fig. 5. PBC-unit cell showing outside periodic image nanotubes in the (2,3)-plane and image atoms in the (1,2)-plane.

conditions. Arrows in Fig. 5a represent the interaction of adjacent nanotubes within the cell and interactions that occur across the boundary with an image cell. A cross-section through the (1,2)-plane depicted in Fig. 5b shows image atoms outside the PBC-unit cell along the axial dimension of the nanotubes.

PBC-unit cells can be constructed of arbitrary order but, with a proper definition of the repeat geometry, the unit energy of the primitive cell remains the same. Therefore the lowest order cell is used for computations. A minimum-order hexagonal PBC-unit cell containing a single nanotube with surrounding image cells is shown in Fig. 6.

The initial equilibrium configuration of the hexagonal unit cell is determined by minimizing the energy of the system as the nanotubes are moved radially outward from a fixed center. This establishes the equilibrium radius, $R_{eq}$, and the nanotube center-to-center separation distance, $S$, as shown in Fig. 7.

The radius of an achiral ($N$, 0) nanotube can be calculated as

$$R_{nt} = \frac{\sqrt{3}}{2\pi} bN \tag{2}$$

where $b$ is the carbon–carbon bond length and $N$ is the number of graphene units around the nanotube circumference.

A rigorous definition of the PBC-unit cell dimensions is required to ensure invariance of the unit energy with cell size. The required planar area of the PBC-unit cell is given by

$$A_{cell} = \frac{3}{2} M\sqrt{3} R_{eq}^2 \tag{3}$$

where $M$ is the number of nanotubes within the cell.

The effective depth of the PBC-unit cell is obtained by first selecting a number of repeat units (circumferential rings of graphene), $K_{seg}$, and adding one additional unit to account for the boundary distance between primary and image segments in the positive and negative axial dimension. Next, as depicted in Fig. 8, the total area of the enclosed graphene units is equated to the surface area of a perfect cylinder having the same radius as the nanotube. This yields a simple expression for the effective depth of the PBC-unit cell given by

$$d_{eff} = \frac{3}{2} b(K_{seg} + 1) \tag{4}$$

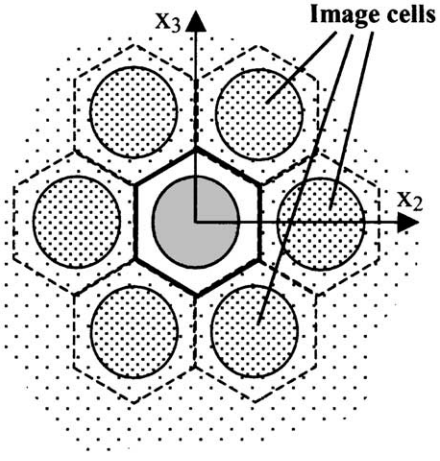


Fig. 6. Minimum hexagonal PBC-unit cell with surrounding image cells.

## 4. Potential energy calculations

The intertube forces are typically modeled by the Lennard–Jones potential to represent van der Waals interactions. The Lennard–Jones or '6–12' potential energy function (Fig. 9) is given by

$$\Phi = 4\varepsilon_{LJ}\left[\left(\frac{\sigma_{LJ}}{r_{ij}}\right)^{12} - \left(\frac{\sigma_{LJ}}{r_{ij}}\right)^{6}\right]. \tag{5}$$

where $\varepsilon_{LJ}$ is the depth of the energy well, $\sigma_{LJ}$ is the van der Waals radius, and $r_{ij}$ is the separation distance between the $i$th and $j$th atoms in a pair. The $r_{ij}^{-6}$ term represents the attractive contribution to the van der Waals forces between neutral molecules. It includes permanent dipole–dipole interactions, the induction

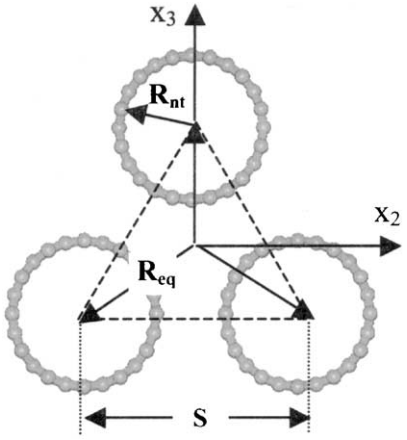


Fig. 7. Equilibrium radius definition for hexagonal cell.

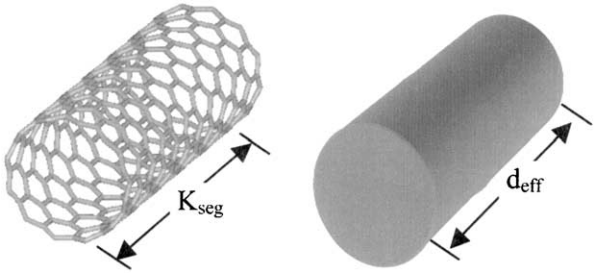


Fig. 8. Effective cylinder length of nanotube.

effect of permanent dipoles, and instantaneous dipole induced dipole interactions which are sometimes referred to as the London dispersion forces. The other component of the van der Waals interactions mimics the repulsion between overlapping electron clouds and is modeled by the $r_{ij}^{-12}$ term which is short ranged [18,19].

## 5. Analysis methodology

The methodology used to determine selected nanotube crystal properties involves defining an appropriate PBC-unit cell, applying selected strain modes to the crystal, and computing the potential energy due to atom-pair interactions as a function of the deformation kinematics. A direct transformation to continuum properties is then made by assuming that the potential energy of discrete atom interactions is equal to the strain energy of a continuous substance occupying the volume of the unit cell.

Effective elastic constants are then determined from the variation in the system strain energy density as

$$C_{ij} = \frac{\partial^2 U_o}{\partial \varepsilon_i \partial \varepsilon_j} \tag{6}$$

where $C_{ij}$ is the material stiffness, $U_o$ is the strain energy density, and $\varepsilon_k$ is an applied strain mode. The original volume is used to compute the energy density, thereby yielding Lagrangian strain measures.

Strain modes are applied to the nanotubes in the crystal by the imposition of specific deformation fields. The $G_{23}$ shear modulus for a hexagonally packed nanotube array is calculated using a PBC-unit cell subjected to a pure shear strain mode as shown in Fig. 10.

The magnitude of the shear strain is given by twice the shear angle or $\gamma_{23} = 2\theta$. During a progressive deformation with increasing $\theta$, the potential energy is computed by summing all atom-pair interactions between adjacent nanotubes at sequencial deformation increments. The $G_{23}$ shear modulus is then obtained from the second derivative of the elastic strain energy density, $U_o$, using a finite difference approximation. This approximation is given by

$$G_{23} = \frac{\partial^2 U_o}{\partial \gamma_{23}^2} = 4\frac{U_{o,i+1} - 2U_{o,i} + U_{o,i-1}}{\left(\gamma_{23,i+1} - \gamma_{23,i-1}\right)^2} \tag{7}$$

where $i$ is the increment in applied strain.

The bulk modulus is computed by applying a dilatational strain as shown in Fig. 11. Because the strain in the axial dimension, $\varepsilon_{11}$, is assumed to be zero, the dilation is defined as $e = \varepsilon_{22} + \varepsilon_{33}$ with $\varepsilon_{22} = \varepsilon_{33} = \varepsilon$. The modulus is then obtained by applying Eq. (7) using a strain given by $2\varepsilon$.

The calculation of the Young's modulus $E_{22}$ and the Poisson's ratio $\upsilon_{23}$ is performed by applying $\varepsilon_{22}$ strain increments in the 2-direction and repositioning the tubes in the 3-direction to minimize the energy. The transverse repositioning of the tubes perpendicular to the load axis directly gives a measure of the $\varepsilon_{23}$ strain from which the

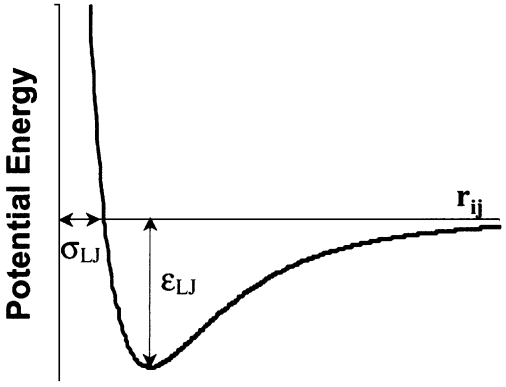


Fig. 9. Shape of the Lennard–Jones potential function.

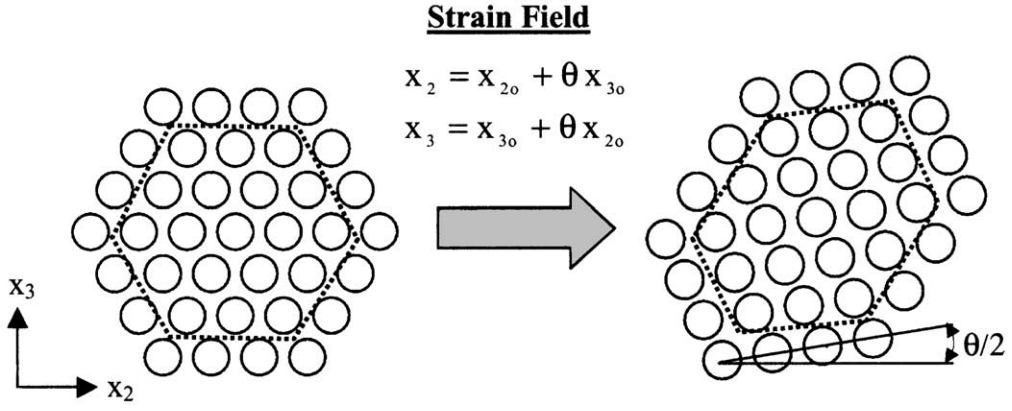


Fig. 10. Imposed shear deformation on hexagonally packed nanotube array.

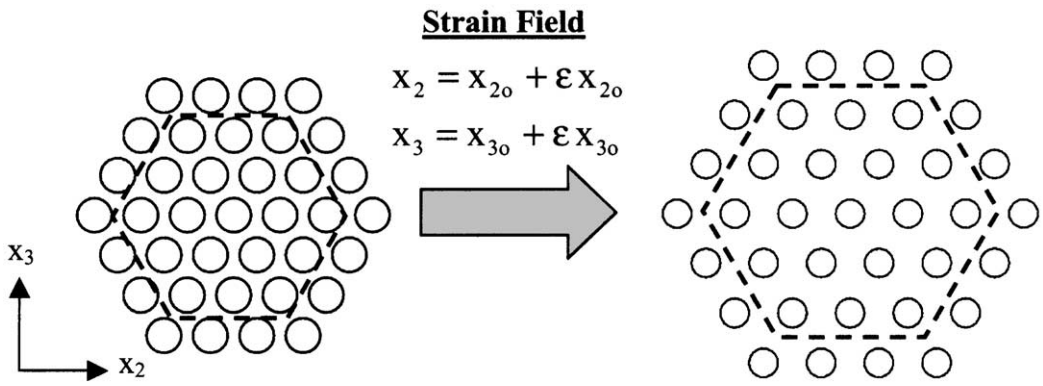


Fig. 11. Imposed dilatational strain on hexagonally packed nanotube array.

Poisson ratio is determined as $\upsilon_{23} = -\varepsilon_{23}/\varepsilon_{22}$. This is depicted in Fig. 12.

The $C_{22}$ stiffness coefficient is obtained by applying the same deformation mode defined in Fig. 12, with no lateral deformation.

## 6. Results and discussion

In the present study, a crystal of identical single-walled nanotubes is analyzed. The carbon–carbon bond length is prescribed as 1.42 Å. All nanotubes were arbitrarily assigned an achiral zig-zag (12,0) conformation with a radius, $R_{nt}$, of 0.471 nm. Equilibrating the system resulted in an equilibrium separation distance of the crystal, $R_{eq}$, of 0.727 nm and a nanotube center-to-center separation distance of 1.26 nm. Nanotubes of this size may be considered rigid in the transverse direction [12,13]. Therefore, the only degree of freedom included in the deformation kinematics is the relative motion of the nanotube center, and the only contribution to the potential energy changes with imposed motion is computed using the Lennard–Jones potential. The parameters used in the Lennard–Jones potential are $\varepsilon_{LJ} = 34$ K and $\sigma_{LJ} = 0.3406$ nm [13,20]. The potential energy of this system in its equilibrium state from the intertube Lennard–Jones contributions alone is 0.57 kcal/mol. For comparison, a single C–C bond has a dissociation energy of 83.1 kcal/mol [24]. A comparison between predicted elastic moduli using the current direct method and results obtained using alternate approaches is presented in Table 1. Refs. [13] and [14] utilize a lattice dynamics approach while Ref. [12] is based on a molecular dynamic simulation. From the limited published results it is clear that there is a wide variation in predicted elastic moduli for nanotube bundles. All the results listed in Table 1 for the present analysis were computed independently, none were derived from a subset of other values.

For a 3-D solid exhibiting hexagonal symmetry, the expression for the transverse Young's modulus, $E_{22}$, is given by [13]

$$E_{22} = \frac{(C_{33} - C_{32})\left[(C_{33} + C_{32})C_{11} - 2C_{31}^2\right]}{\left(C_{33}C_{11} - C_{13}^2\right)} \tag{8}$$

Because the axial modulus of the nanotubes in the crystal is generally two orders of magnitude greater than

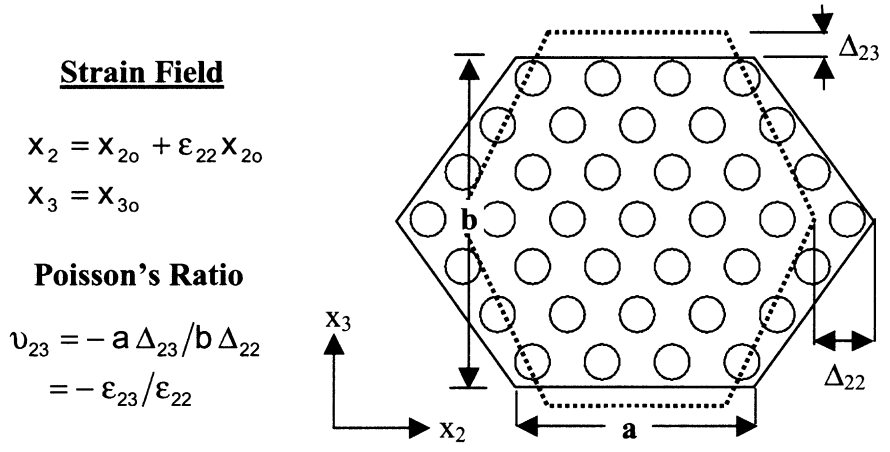


Fig. 12. Calculation of Poisson's ratio.

the transverse moduli, we may take $C_{11} >> C_{33}$, $C_{32}$, $C_{31}$. Using the relationship $C_{23} = \upsilon_{23} C_{22}$ and equating Poisson ratios under transverse plane isotropy as $\upsilon_{23} = \upsilon_{32}$, Eq. (8) reduces to a simple relationship between $C_{22}$, $E_{22}$ and $\upsilon_{23}$. Substituting the calculated values for the Young's modulus $E_{22}$ and Poisson's ratio $\upsilon_{23}$ into the resulting expression, the transverse normal stiffness is obtained as

$$C_{22} = \frac{E_{22}}{1 - \upsilon_{23}^2} = \frac{60.3}{1 - 0.34^2} = 68.2 \text{ GPa} \tag{9}$$

which closely agrees with the independently calculated value of $C_{22}$ in Table 1. Next, computing $C_{23}$ as $\upsilon_{23} C_{22} = 23.2$ GPa and applying the relations given by Eq. (1), it is found that the transverse plane stiffnesses are recoverable from the computed shear and bulk moduli as

$$C_{22} = K_{23} + G_{23} = 45.8 + 22.5 = 68.3 \text{ GPa} \tag{10}$$

$$C_{23} = K_{23} - G_{23} = 45.8 - 22.5 = 23.3 \text{ GPa}$$

Thus, the computed elastic constants are completely self-consistent for a transversely isotropic material as expected due to hexagonal symmetry. The values reported in Ref. [13] (Table 1) are also self-consistent for transverse isotropy and compare favorably with the present analysis for the prediction of the bulk modulus, $K_{23}$. The results from a molecular dynamics simulation presented in Ref. [12] (Table 1) are slightly lower. The calculation of the normal stiffness, $C_{22}$, which is obtained from applying a similar deformation as that used to compute the bulk modulus (applying only $\varepsilon_{22}$ instead of both $\varepsilon_{22}$ and $\varepsilon_{33}$), is intermediate between the lattice dynamics studies presented in Refs. [13] and [14] (Table 1). In Ref. [14] nanotubes of the same radius were used but with different chirality. However, the effect of chirality is discussed in Ref. [13] in which it is shown for several cases that the configuration of graphene units on the nanotube surface has a negligible effect for small radius tubes ($R < 16$ Å).

The $C_{23}$ value derived here using $G_{23}$ and $K_{23}$ in Eq. (10) or $E_{22}$ and $\upsilon_{23}$ in Eq. (9) are self-consistent and yield a value of 23 GPa. The only other available comparison for $C_{23}$ is in Ref. [13] which presents a value of 32 GPa. Another value not reported in the literature is the transverse shear modulus $G_{23}$ for which the present analysis yields 22.5 GPa. This value varies from 20.2 GPa to 24.7 GPa with 10% variation in the Lennard–Jones $\sigma_{LJ}$ and $\varepsilon_{LJ}$ parameters. If one applies the first of the relations given in Equations (1) to the data in Ref. [13], one obtains a value for $G_{23}$ of 5.3 GPa. This lower value of the shear modulus is comparable to the shear modulus associated with parallel planes in graphite, which is experimentally measured as 4.0 GPa [21,22].

Table 1
Comparison of predicted elastic constants

| Elastic constant | Direct method | Popov [13] | Lu [14][b] | Tersoff [12] |
|---|---|---|---|---|
| Bulk modulus $K_{23}$ (GPa) | 45.8 | 42.0 | 18.0 | 33.6 |
| Shear modulus $G_{23}$ (GPa) | 22.5 | 5.3[a] | – | – |
| Young's modulus $G_{23}$ (GPa) | 60.3 | 17.0 | – | – |
| Normal stiffness $C_{22}$ (GPa) | 68.3 | 42.0 | 78.0 | – |
| Poisson ratio $\nu_{23}$ | 0.34 | 0.75 | – | – |

[a] Value derived using relationship in Eq. (1).
[b] Results generated using (7,7) chiral nanotubes with diameter = 0.94 nm.

In the direct summation and lattice dynamic methods, the physics of cohesion are identically represented by the same parameterization of the Lennard–Jones potential. Possible differences in predictions using lattice dynamics may be due to the inherent integral averaging of force constants used in the lattice dynamical matrix and the a priori selection of interacting nearest-neighbor atoms used in defining the primitive lattice cell, both of which are avoided in the direct method.

A potential source of inaccuracy affecting all methods is the form of the Lennard–Jones potential function itself. The Lennard–Jones potential was originally developed for noble gases and is known to produce poor results in other applications including graphite. It gives good results for the $C_{33}$ modulus (interplanar separation), but the $C_{44}$ parallel plane shear modulus is under-predicted by an order of magnitude [22]. Alternative potentials have been proposed [23] that yield accurate predictions for both the transverse normal and shear moduli in graphite. Additional study is warranted to assess the spatial interactions of delocalized bonds in carbon nanotubes that may be underestimated using a spherical Lennard–Jones model.

The developed analysis has been applied to the prediction of transverse mechanical moduli of perfect carbon nanotube crystals. Due to the highly nonlinear van der Waals cohesion between carbon nanotubes, the effect of lattice defects may be expected to have a significant impact on transverse bundle properties. This issue together with some additional comments regarding the use of the Lennard–Jones potential is presented in a companion paper [26].

## 7. Concluding remarks

A consistent method has been formulated for and applied to computing effective transverse mechanical properties of nanotube crystals. The method is based on specifying a unit cell configuration with periodic boundary conditions, applying a deformation field associated with a particular strain mode, and utilizing a direct summation procedure to compute changes in potential energy from which an effective elastic modulus

may be obtained. For the present analysis, the disparity between reported predictions of mechanical properties that depend exclusively on van der Waals cohesion and the paucity of available experimental data suggest that much additional investigation is warranted in this area. The development of a more realistic representation of van der Waals interactions between nanotube surfaces may be required to correlate analytical predictions with future experimental measurements of nanotube crystal properties.

## Acknowledgements

The authors would like to thank Professor V. Popov at the University of Sofia for helpful discussions during the course of this work. S.J.V. Frankland was supported by the National Aeronautics and Space Administration under NASA Contract No. NAS1-97046 while in residence at ICASE, NASA Langley Research Center, Hampton, VA 23681-2199, USA.

## References

[1] Thess A, Lee R, Nikolaev P, Dai H, Petit P, Robert J, et al. Crystalline ropes of metallic carbon nanotubes. Science 1996;273:483–7.
[2] Salvetat JP, Briggs GAD, Bonard JM, Bacsa RR, Kulik AJ, Stockli T, et al. Elastic and shear moduli of single-walled carbon nanotubes. Phys Rev Lett 1999;82:944–7.
[3] Krishnan A, Dujardin E, Ebbesen TW, Yianilos PN, Treacy MMJ. Young's modulus of single-walled nanotubes. Phys Rev B 1998;58:14013–9.
[4] Sanchez-Portal D, Artacho E, Soler JM, Rubio A, Ordejon P. *Ab initio* Structural, elastic, and virbrational properties of carbon nanotubes. Phys Rev B 1999;59:12678–88.
[5] Hernandez E, Goze C, Bernier P, Rubio A. Elastic properties of C and $B_xC_yN_z$ composite nanotubes. Phys Rev Lett 1998;80:4502–5.
[6] Cornwell CF, Wille LT. Elastic properties of single-walled carbon nanotubes in compression. Solid State Commun 1997;101:555–8.
[7] Popov VN, Van Doren VE, Balkanski M. Elastic properties of single-walled carbon nanotubes. Phys Rev B 2000;61:3078–84.
[8] Lu JP. Elastic properties of single and multilayered nanotubes. J Phys Chem Solids 1997;58:1649–52.
[9] Frankland SJV, Caglar A, Brenner DW, Griebel M. Molecular simulation of the influence of chemical cross-links on the shear strength of carbon nanotube-polymer interfaces. J Phys Chem B 2002;106:3046–8.
[10] Pipes RB, Hubert P. Helical carbon nanotube arrays: mechanical properties. Comp Sci Tech 2002;62:419–28.
[11] Girifalco LA, Hodak M, Lee RS. Carbon nanotubes, buckyballs, ropes, and a universal graphitic potential. Phys Rev B 2000;62: 13104–10.
[12] Tersoff J, Ruoff RS. Structural properties of a carbon-nanotube crystal. Phys Rev Lett 1994;73:676–9.
[13] Popov VN, Van Doren VE, Balkanski M. Elastic properties of crystals of single-walled carbon nanotubes. Solid State Commun 2000;114:395–9.
[14] Lu JP. Elastic properties of carbon nanotubes and nanoropes. Phys Rev B 1997;79:1297–300.
[15] Theodorou DN, Suter UW. Atomistic modeling of mechanical properties of polymeric glasses. Macromolecules 1986;19:139–54.
[16] Fan CF, Hsu SL. Application of the molecular simulation technique to characterize the structure and properties of an aromatic polysulfone system. 2 Mechanical and thermal properties. Macromolecules 1992;25:265–70.
[17] Hashin Z, Rosen BW. The elastic moduli of fiber-reinforced materials. J Appl Mech 1964;June:223–32.
[18] Allen MP, Tildesley DJ. Computer simulation of liquids. Clarendon Press; 1987.
[19] Moore WJ. Physical Chemistry. 4th ed. Englewood Cliffs (NJ): Prentice Hall; 1972. p. 913–4.
[20] Lu JP, Yang W. The shape of large single- and multiple-shell fullerenes. Phys Rev B 1994;49:11421–4.
[21] Kelly BT, Duff MJ. On the validity of Lennard-Jones potentials for the calculation of elastic properties of a graphite crystal. Carbon 1970;8:77–85.
[22] Green JF, Bolland TK, Bolland JW. Lennard–Jones interactions for hexagonal layered crystals. J Chem Phys 1974;61:1637–46.
[23] Kolmogorov AN, Crespi VH. Smoothest bearings: interlayer sliding in multiwalled carbon nanotubes. Phys Rev Lett 2000;85: 4727–30.
[24] Pauling L. The nature of the chemical bond. 3rd ed. Ithaca (NY): Cornell University Press; 1960. p. 85.
[25] Hamada N, Sawada SI, Oshiyama A. New one-dimensional conductors: graphitic microtubules. Phys Rev Lett 1992;68:1579–81.
[26] Saether, E. Transverse mechanical properties of single-walled carbon nanotube crystals. Part II: sensitivity to lattice distortion. Comp. Sci. Technol. [in press].